Foraminiferal responses to major Pleistocene paleoceanographic changes in the southern South China Sea

Zhimin Jian, Pinxian Wang, Min-Pen Chen, Baohua Li, Quanhong Zhao, Christian Bühring, Carlo Laj, Hui-Ling Lin, Uwe Pflaumann, Yunhua Bian, et al.

PALEOCEANOGRAPHY, VOL. 15, NO. 2, PAGES 229-243, APRIL 2000

Foraminiferal responses to major Pleistocene paleoceanographic changes in the southern South China Sea

Zhimin Jian,[1,2] Pinxian Wang,[1] Min-Pen Chen,[3] Baohua Li,[4] Quanhong Zhao,[1] Christian Bühring,[5] Carlo Laj,[6] Hui-Ling Lin,[7] Uwe Pflaumann,[5] Yunhua Bian,[1] Rujian Wang[1] and Xinrong Cheng[1]

Abstract. A detailed age model for core 17957-2 of the southern South China Sea was developed based on $\delta^{18}O$, coarse fraction, magnetostratigraphy, and biostratigraphy for the last 1500 kyr. The $\delta^{18}O$ record has clear ~100-kyr cycles after the Mid-Pleistocene Revolution (MPR) at the entrance of marine isotopic stage (MIS) 22. Planktonic foraminifera responded to the MPR immediately, showing the increased sea surface temperature (SST) and dissolution after the MPR. Benthic foraminifera did not respond to it until the Brunhes/Matuyama boundary. Since the MPR, the depth of thermocline gradually became shallower until MISs 6-5. This major change within MISs 6-5 was also reflected in the decreased SSTs and increased productivity and Deep Water Mass. Thus two major Pleistocene paleoceanographic changes were found: One was around the MPR; the other occurred within MISs 6-5, which speculatively might be ascribed to the reorganization of surface and deep circulation, possibly induced by tectonic forces.

1. Introduction

As a marginal sea the South China Sea (SCS) has sedimentation rates higher by an order of magnitude than the Pacific, and its widespread carbonate sediments provide an ideal basis for high-resolution paleoceanographic reconstruction [*Wang et al.*, 1995]. The first cores in the world ocean used for high-resolution stratigraphy documented by accelerator mass spectrometer (AMS) ^{14}C datings were from the southern part of this basin [*Andree et al.*, 1986; *Broecker et al.*, 1988]. Since the 1980s, marine geologists in China and abroad have shown growing interest in late Quaternary paleoceanographic history of the SCS, for example, the changes in sea surface temperature (SST) [*Wang and Wang*, 1990; *Miao et al.*, 1994; *Pflaumann and Jian*, 1999], productivity [*Winn et al.*, 1992; *Thunell et al.*, 1992; *Jian et al.*, 1999], deepwater conditions [*Berger*, 1987; *Jian and Wang*, 1997], carbonate cycles [*Wang et al.*, 1986; *Thunell et al.*, 1992; *Wang et al.*, 1995], monsoon variations [*Sun and Li*, 1999; *Wang et al.*, 1999], and paleoenvironmental interactions between land and sea [*Wang and Sun*, 1995; *Wang*, 1999] during the last glacial-interglacial cycle. On the other hand, the high sedimentation rate in the SCS has hindered the Pleistocene paleoceanographic studies because no core has penetrated the last two glacial cycles. The long come from industrial exploratory wells, engineering geological drill holes and coral reef deposits, which hardly provide continuous and detailed paleoenvironmental records [e.g., *Zhang et al.*, 1996]. Therefore long-term Pleistocene paleoenvironmental records from the China coast are not yet available to be compared with those recorded in the Chinese loess [*Kukla and An*, 1989; *Liu and Ding*, 1993; *Ding et al.*, 1994], despite their primary importance in our understanding of the East Asian paleoenvironmental evolution.

The surface water masses and hydrography in the SCS are largely controlled by the seasonally reversing monsoonal wind system, which causes drift currents to change their flow direction [*Wyrtki*, 1961]. According to *Levitus and Boyer* [1994], the SST of the SCS ranges from 20° to 28.8°C during the northeast winter monsoon, with steep gradients toward the coast of China. During the southwest summer monsoon, the SST varies only from 27° to 29°C. The annual average depth of thermocline (DOT) in the SCS ranges from ~25 m in the inner shelf to ~200 m toward the western Pacific, primarily responding to the wind-driven cyclonic surface circulation (i.e., Ekman pumping). For more detailed information on the modern geographic variations of the SSTs and DOT in the SCS, see *Chen et al.* [1998] and *Pflaumann and Jian* [1999]. However, during the glacial period the SCS became a semienclosed basin connected to the western Pacific through the Bashi Strait and to the Sulu Sea through the Balabac and Mindoro Straits due to the sea level drop [*Wang et al.*, 1995]. This inevitably led to a pronounced difference in surface and deep circulation [*Wang et al.*, 1995; *Jian and Wang*, 1997] and hence altered the upper water structure and deep water conditions.

The northern part of Nansha Islands area ("Dangerous Ground"), the northern slope of the SCS deep basin, is

[1]Laboratory of Marine Geology, Tongji University, Shanghai, China.
[2]Now at Institut für Geowissenschaften, Universität Kiel, Kiel, Germany
[3]Institute of Oceanography, Taiwan University, Taipei, China.
[4]Nanjing Institute of Geology and Paleontology, Academia Sinica, Nanjing, China.
[5]Institut für Geowissenschaften, Universität Kiel, Kiel, Germany.
[6]Laboratoire des Sciences du Climat et de l' Environment, CNRS-CEA, Gif sur Yvette, France.
[7]Institute of Marine Geology, Sun Yat-Sen University, Kaohsiung, Taiwan, China.

Paper number 1999PA000431.
0883-8305/00/1999PA000431$12.00

distinguished by its very low sedimentation rate because of the limited access of terrigenous material and may provide continuous and long Pleistocene deep-sea sediment sequences [*Sarnthein et al.*, 1994; *Wang et al.*, 1995]. Moreover, this area offers a special attraction for paleoceanographers, with only slight seasonality in SST and modern annual DOT of ~175 m [*Levitus and Boyer*, 1994]. Particularly, the southern SCS is a part of the Western Pacific Warm Pool (WPWP) bounded approximately by the 28°C surface isotherm [*Yan et al.*, 1992]. Its long-term changes in upper water structure perhaps have influenced the thermodynamics role played by the WPWP. In this study we selected a long deep-sea core with good carbonate preservation from the southern SCS to establish a detailed stratigraphy at least for the last 1500 kyr through an interdisciplinary approach, including magnetostratigraphy, biostratigraphy, oxygen isotope, and coarse fraction stratigraphy. By examining paleoceanographic records from the core we were able to reveal the planktonic and benthic foraminiferal responses to major Pleistocene paleoceanographic changes, for example, the Mid-Pleistocene Revolution (MPR) near 900 ka [*Berger et al.*, 1993a], and to get insight into the changes of surface and deep circulation during the Pleistocene in the SCS.

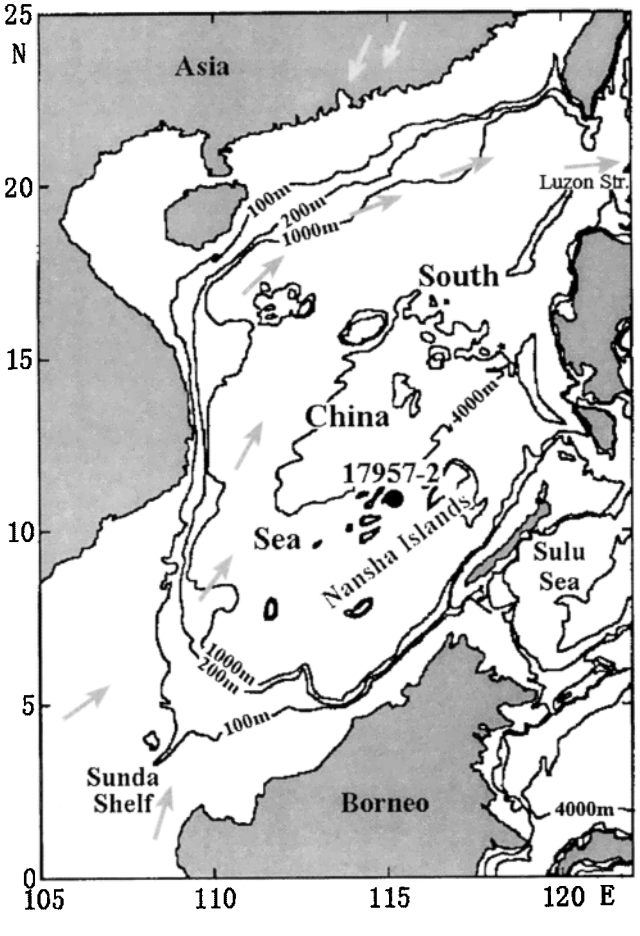

Figure 1. Location of core 17957-2 in the South China Sea. Gray arrows show modern surface currents during summer; white arrows show winter monsoon.

Table 1. Sample Information of Core 17957-2 Used in This Study

Analytical Item	Sample Interval, cm	Number of Samples
Planktonic foraminifera	5	272
Benthic foraminifera	10	136
Calcareous nannofossil	20	51
Radiolarian	10	136
Stable isotope	10	138
Coarse fraction	5	273
Carbonate	10	139
Opal	5	272

2. Material and Methods

We studied gravity core 17957-2 raised from the southern SCS, north of the Nansha Islands (10°53.9'N and 115°18.3'E; water depth 2195 m; core length 1384 cm) (Figure 1) during the SONNE-95 cruise in 1994 [*Sarnthein et al.*, 1994]. The sediment in the core consists of gray silty foraminiferal ooze free of turbiditic (or mass flow) deposition and major reworking. The core was sampled at 5-20-cm intervals, according to individual analytical item (Table 1). Three to ten cubic centimeters of wet sediment were dried and weighed for each sample while coarse fraction content was obtained through wet sieving over a 63-μm screen. Planktonic and benthic foraminifera were picked only from the size fraction ≥ 150 μm. When planktonic foraminifera were abundant, the sample was split using biseparation method to yield a subsample containing at least 300 specimens.

Planktonic and benthic foraminifera were identified and counted. Our taxonomy follows that of *Parker* [1962], *Bé* [1977], and *Kennett and Srinivasan* [1983] for planktonic foraminifera and that of *Barker* [1960] and *Loeblich and Tappen* [1988] for benthic foraminifera. On the basis of the census data the relative abundance of each species was calculated and plotted against depth to illustrate the down-core distribution patterns. We estimated the SSTs using two different planktonic foraminiferal transfer functions. The standard errors of the linear transfer function FP-12E [*Thompson*, 1981] are 2.48°C for winter SST and 1.46°C for summer SST, while those of the SIMMAX-28 formula using modern analog technique [*Pflaumann and Jian*, 1999] are 1.27° and 0.45°C, respectively. For the first time we used the thermocline depth transfer function of *Andreasen and Ravelo* [1997], which was based on the spatial distribution of 189 core top planktonic foraminifera in the tropical Pacific, to quantitatively reconstruct the changes of DOT in the SCS during the Pleistocene glacial cycles. This transfer function has a standard error of 22 m and additional 5 m of error due to insufficient counts in the core top database [*Andreasen and Ravelo*, 1997]. As for the benthic foraminifera, a *Q* mode factor analysis was carried out using the program of *Klovan and Imbrie* [1971]. Only species with relative abundance >2% in at least two samples (48 species and species groups, see Table 3) were included in the factor analysis. Carbonate dissolution/preservation was evaluated using changes in planktonic foraminiferal fragmentation, benthic foraminiferal proportion (expressed as BF/(BF+PF)%, where BF and PF are benthic and planktonic foraminiferal abundance, respectively), and the percentage of agglutinated tests in benthic foraminiferal fauna. Fragmentation is expressed as fragmentation =

$(F/8)/(F/8+W)$%, where F is the number of fragments and W is that of well-preserved planktonic foraminifera in the sample [*Le and Shackleton*, 1992]. Calcareous nannofossil and radiolarian were analyzed only for providing biostratigraphic controls in this study and will be discussed in separate papers later.

Determination of carbonate content in the sample was made at Taiwan University according to the weight loss method outlined by *Molnia* [1974]. The salt in each sample was, however, washed out by distilled water before the carbonate material was dissolved by 1 *N* hydrochloric acid. Opal content was measured at Sun Yat-Sen University in Kaohsiung following the technique of *Mortlock and Froelich* [1989] with slight modifications described by *Murray et al.* [1993], except that 0.5 *N* NaOH instead of 2 *M* Na_2CO_3 was used to extract the biogenic opal. Overall, the analytical precision of the carbonate and opal determination are better than 1.0 and 1.5%, respectively.

Oxygen and carbon stable isotope measurements were carried out on the planktonic foraminiferal species *Globigerinoides sacculifer* (wo) (without a saclike final chamber) (>150 μm) using a V. G. Micromass 602 mass spectrometer at the Institute of Earth Sciences, Academia Sinica at Taipei. The analytical precision expressed as 1σ for NBS-19 standard carbonate was 0.06‰. The average difference of duplicate foraminiferal analyses is ~0.12‰ for oxygen and 0.09‰ for carbon.

High-resolution continuous paleomagnetic measurements were performed at the Laboratoire des Sciences du Climat et de l' Environment (LSCE) of the Centre National de la Recherche Scientifique (CNRS)-Commissariat à l' Energie Atomique (CEA), France. The sediments were sampled using the 1-m-long u channel plastic container [*Tauxe et al.*, 1983; *Weeks et al.*, 1993]. The natural remnant magnetization was measured continuously with a resolution of ~3 cm using a pass-through DC-SQUID cryogenic magnetometer in a shielded room. Stepwise in-line demagnetization with an average of 8-10 steps up to 60 mT was used to retrieve the primary component of the magnetization, which was isolated after the very first steps of demagnetization.

For spectral analyses a menu-driven PC program SPECTRUM [*Schulz and Stattegger*, 1997] was used. Compared to the widely used Blackman-Turkey approach for spectral analysis, the advantage of SPECTRUM is the avoidance of any interpolation of the time series. The interpolation of unevenly spaced time series may significantly bias statistical results because the interpolated data points are no longer independent [*Schulz and Stattegger*, 1997]. In this study, we selected 1.0 and 4.0 for the highest frequency factor (HIFAC) and the oversampling factor (OFAC), respectively, for a good compromise between computing time and smoothness of a spectrum. The time series was divided into three 50% overlapping Welch-overlapped-segment-averaging (WOSA) segments which were linearly detrended.

The material used in this study is stored at the Laboratory of Marine Geology, Tongji University. The complete data discussed in this paper are available upon request.[1]

Table 2. Microfossil Datums and Magnetostratigraphic Events Adopted in This Study

Stratigraphic Events	Depth, cm	Age, Ma	Reference
Pink *Globigerinoides ruber* LAD	180	0.12	1
Pseudoemiliania lacunosa LAD	560	0.46	2
Stilostomella Extinction	690	0.62	3
Brunhes/Matuyama Boundary	795	0.78	4, 5
Top Jaramillo	967	0.99	4, 5
Base Jaramillo	1020	1.07	4, 5
Anthocyrtidium angulare LAD	1080	1.15	6, 7
Cobb Mountain	1120	1.201-1.211	4, 5

LAD is last appearance datum. (1) *Thompson et al.* [1979]; (2) *Thierstein et al.* [1977]; (3) *Schönfeld* [1996]; (4) *Shackleton et al.* [1990]; (5) *Berggren et al.* [1995]; (6) *Moore* [1995]; (7) *Shackleton et al.* [1995].

3. Results

3.1. Chronological Framework

First, a low-resolution chronological framework was developed on the basis of microfossil biostratigraphy and magnetostratigraphy for the last 1500 kyr. Four datums of calcareous and siliceous microfossils, including planktonic and benthic foraminifera, calcareous nannofossil, and radiolarian, were adopted in this study (Table 2). The Brunhes/Matuyama (B/M) magnetic polarity reversal (0.78 Ma) is clearly apparent as a change to negative inclination and a 180 swing of the declination at a depth of 795 cm. The upper Jaramillo (0.99 Ma) transition, unfortunately coinciding with the separation between two u channels, is around 967 cm. The lower Jaramillo (1.07 Ma) transition is situated at a depth of 1020 cm, again characterized by a change to negative inclination and a declination swing. The sharp swing in declination at 1120 cm might correspond to the Cobb Mountain event (between 1.201 and 1.211 Ma) (Figures 2 and 3 and Table 2).

Of particular interest is the discovery of microtektites at the depths of 780-815 cm, with conspicuous peak at the depths of 805-810 cm slightly below the B/M boundary (Figure 3) [*Zhao et al.*, 1999]. According to its chemical and physical properties, the microtektites in the core also occurred extensively in deep sediments of Australasian area [*Glass*, 1967; *Smit et al.*, 1991] and Chinese loess [*Wu et al.*, 1992]. It therefore can serve as an additional stratigraphic marker in the SCS. Time-to-depth conversions (Figure 2) were performed by assuming constant sedimentation rates between the biostratigraphic and magnetostratigraphic control points (Table 2), which shows no obvious hiatus in the core during the last 1500 kyr. The estimated average sedimentation rate for the core is ~0.93 cm/kyr.

We constructed more detailed age model primarily based on foraminiferal $\delta^{18}O$ and coarse fraction records, with constraints of biostratigraphic and magnetostratigraphic control points (Figure 3). The chronology for the isotopic age model was developed from ODP Site 677 [*Shackleton et al.*, 1990], different from those proposed by *Ruddiman et al.* [1989]. Coarse fraction stratigraphy developed in the equatorial Indian Ocean [*Bassinot et al.*, 1994]

[1] Supporting data are available on diskette or via Anonymous FTP from www.agu.org, directly APEND (username = anonymous, Password = guest). Diskette may be ordered from American Geophysical Union, 2000 Florida Avenue, N.W., Washington, DC 20009 or by phone at 800-966-2481; $15.00. Payment must accompany order.

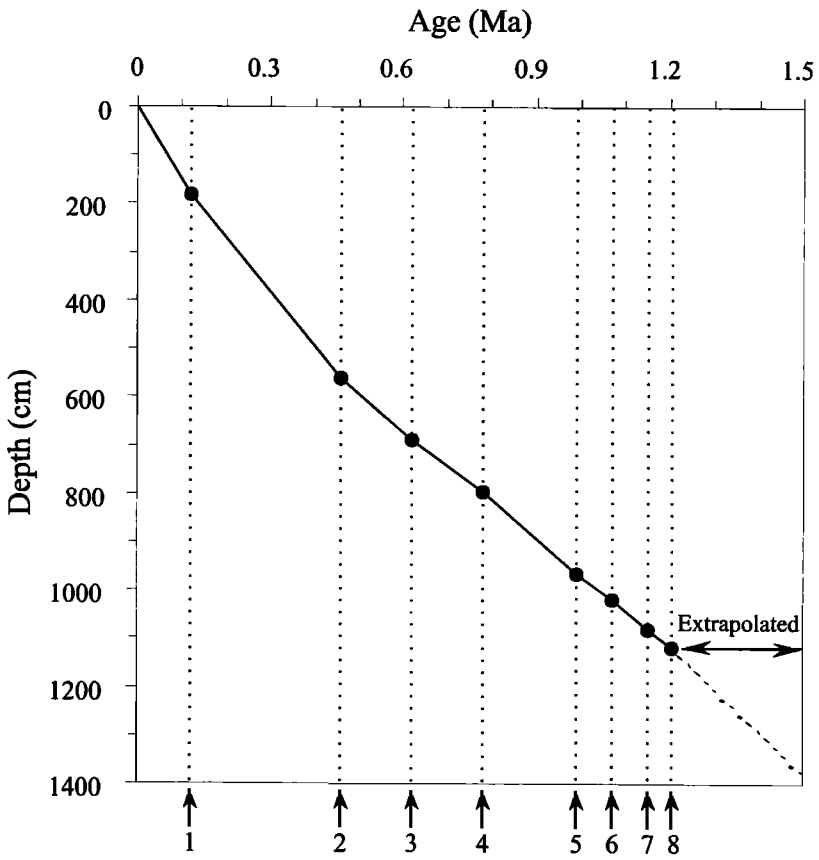

Figure 2. Age-depth plot showing sedimentation rates in core 17957-2: 1, pink *Globigerinoides ruber* last appearance datum (LAD); 2, *Pseudoemiliania lacunosa* LAD; 3, *Stilostomella* extinction; 4, Brunhes/Matuyama boundary; 5, top of Jaramillo; 6, base of Jaramillo; 7, *Anthocyrtidium angulare* LAD; 8, Cobb Mountain event.

was applied in the SCS. Major peaks (CF2~23) of the coarse fraction curve in core 17957-2 have been labeled according to their position relative to the $\delta^{18}O$ stratigraphy (Figure 3), which can be well correlated with those from ODP Site 758 in the Indian Ocean. The age of each sample was interpolated on the basis of the average sedimentation rate between the isotopic age model control points. The base of the core reaches ~1.50 Ma.

The most striking change for $\delta^{18}O$ and coarse fraction curves is the MPR at the entrance to glacial marine isotopic stage (MIS) 22 [*Berger et al.*, 1993a]. After this time, the eccentricity cycles of ~100 kyr entirely dominated. Before it, the low-amplitude obliquity cycles of 41 kyr is more important. Taking the records at face value, little or no evidence exists for a transition zone: the change is abrupt, at least on the timescale considered here (Figure 3). Thus, back to the Cobb Mountain event, the stratigraphy of this core is reliable, while a minor hiatus or extremely low sedimentation rate occurs between MISs 22 and 24 and between MISs 27 and 29 (Figure 3). Below it, however, the recognition of MIS is relatively difficult without biostratigraphy and magnetostratigraphic controls.

3.2. Variations in the Sea Surface Temperature

Variations in the relative abundance of main planktonic foraminiferal species which could be divided into shallow- and deep-dwelling species [*Bé*, 1977; *Fairbanks et al.*, 1982; *Ravelo et al.*, 1990] were examined (Figures 4 and 5). MISs 22-20 from the MPR to B/M boundary and MISs 6-5 are two important boundaries. During MISs 6-5 the abundances of tropical-subtropical species *Globigerinoides ruber* and *G. sacculifer* (wo) remarkably decreased, while those of temperate species *Neogloboquadrina dutertrei* and *Globorotalia crassaformis* reached maximum, indicating a considerable decrease in SSTs. After MISs 22-20, the abundances of shallow-dwelling species *G. ruber*, *G. sacculifer* (wo) and *Globigerina bulloides* decreased, while those of deep-dwelling species *Pulleniatina obliquiloculata*, *Globorotalia menardii*, *G. crassaformis*, and *Globorotalia inflata* remarkably increased. Nevertheless, all the species in Figures 4 and 5 except *G. inflata* have no clear consistent glacial-interglacial changes.

Planktonic foraminifera in the core are well preserved with low fragmentation (<10%; see Figure 9), and the estimated SSTs using two different techniques have very low correlation (R^2<0.01) with the fragmentation, indicating that the temperature estimates are not biased by carbonate dissolution. All planktonic foraminiferal species except pink *G. ruber* in the core can be found in surface sediments of the western pacific and SCS [*Thompson*, 1981; *Pflaumann and Jian*, 1999]. Even pink *G. ruber* took only a small part of *G. ruber* during the period of ~400-120 ka [Li, 1997]. The evolutionary changes therefore could not much influence the SST estimates during the last 1500 kyr in the SCS.

The estimated SSTs of core top from FP-12E and SIMMAX-28 are 27.2° and 27.0°C for winter, and 29.4° and 28.9°C for summer, respectively. Their differences with the present day SSTs at this site (27.03°C for winter and 28.85°C for summer [*Levitus and Boyer*, 1994]) are less than the standard errors of estimation [*Thompson*, 1981; *Pflaumann and Jian*, 1999]. The SIMMAX-28-derived winter SST ranges from 24.7° to 27.8°C, averaging 27.0°C, while the SIMMAX-28-derived summer SST changes little from 28.8° to 29.4°C with an average of 29.0°C (Figure 6a). Their amplitudes of fluctuation are much greater than the standard errors of SIMMAX-28, indicating the changes of SIMMAX-28-derived SSTs are quite reliable. As for the FP-12E-derived SSTs, the winter SST ranges from 24.5° to 27.8°C, averaging 26.4°C, while the summer SST changes little from 28.7° to 30.0°C with an average of 29.3°C (Figure 6b). The amplitude of fluctuation in the FP-12E-derived winter SST (3.3°C) is greater than the standard error of the FP-12E cold equation, implying that the changes of FP-12E-derived winter SST are really significant.

Compared to previous data in the SCS using the transfer function FP-12E [*Wang and Wang*, 1990; *Miao et al.*, 1994; *Wang et al.*, 1995], both the estimated winter and summer SSTs from FP-12E and SIMMAX-28 are slightly warmer with a narrower range of seasonality in core 17957-2. This may be explained by the fact that (1) the core is located in the tropical SCS as a part of WPWP and (2) it is far away from the influence of coastal currents. As shown in Figure 6a, the SIMMAX-28-derived winter SST changed little after the B/M boundary, except the excursions at MISs 7/8 and during MISs 6-5. However, before the boundary, it was very changeable with four distinct decreases. The average SIMMAX-28-derived winter SST before the B/M boundary is 26.7°C, lower than the average value of 27.2°C after it. However, the greatest change in the FP-12E-derived winter SST occurred at MISs 21/22, which divides the curve into two clear sections. The average FP-12E-derived winter SST was 26.6°C after MIS 21, while it was only 26.1°C before the time (Figure 6b). on the basis of the results from two different transfer functions the tropical SSTs slightly increased right after the obvious decrease in winter SST during MISs 22-20, which may correspond to the climate changes at the MPR [*Berger et al.*, 1993]. Since the B/M boundary, the winter SST changed within a range of <3°C, in agreement with those of *Climate: Long-Range Investigation, Mapping, and Prediction* (*CLIMAP*) *Project Members* [1981] in the western equatorial Pacific. This further supports that "the last 1.0 Ma was dominantly a period of lower SST in the late Neogene, except at the tropics where SST was a little higher than before and experienced only minor fluctuations in the western Pacific,"

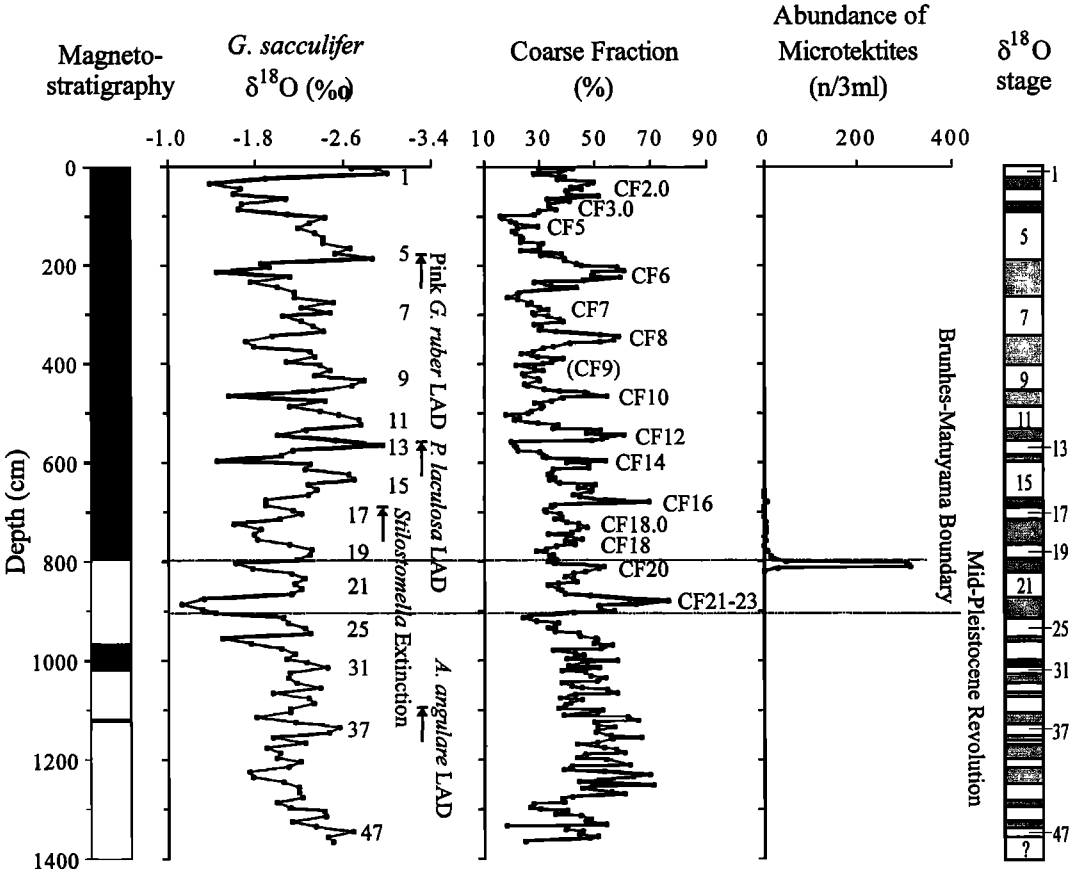

Figure 3. Magnetostratigraphic, oxygen isotopic, and coarse fraction stratigraphic framework in core 17957-2. The magnetostratigraphy is shown as a column with the usual black and white convention for normal and reverse periods, respectively. Major peaks of the coarse fraction curve (CF2~23) have been labeled according to their position relative to the $\delta^{18}O$ stratigraphy [*Bassinot et al.*, 1994]. The biostratigraphic and microtektite control points are also shown. Marine oxygen isotopic stages are indicated on the right side.

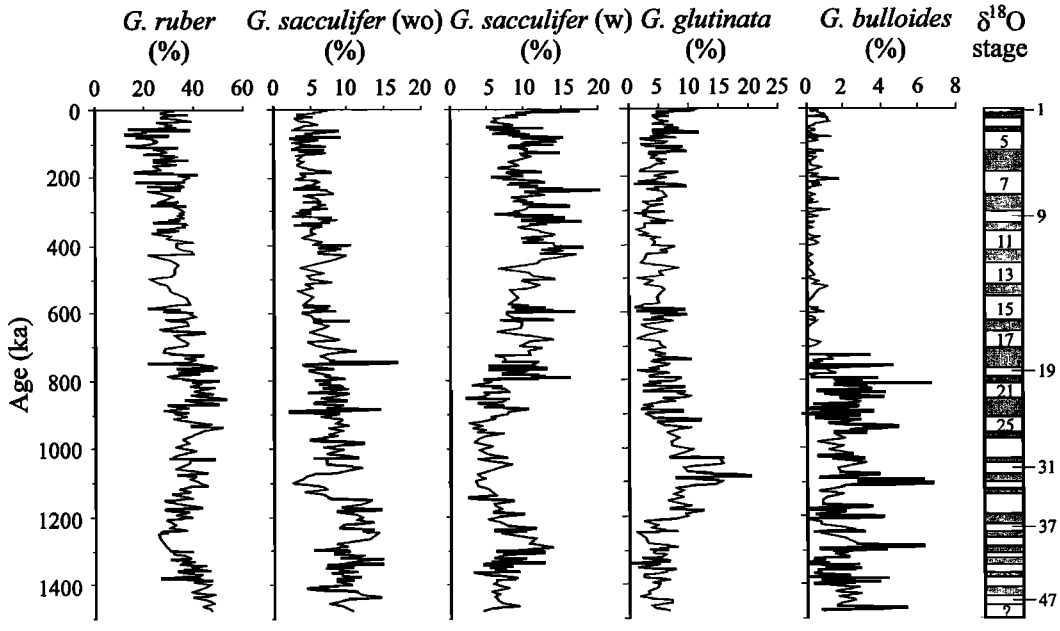

Figure 4. Variations in relative abundance of selected shallow-dwelling planktonic foraminiferal species. *G. sacculifer* (w) is *G. sacculifer* with a saclike final chamber. Marine oxygen isotopic stages are indicated on the right side.

concluded by *Wang* [1994, p. 379]. It seems that the WPWP was relatively stable during the late Pleistocene glacial cycles [*Thunell et al.*, 1994]. However, there was an obvious decrease in the winter SST during MISs 6-5, judging from the FP-12E-derived and SIMMAX-28-derived curves (Figure 6). This event made the winter SST higher during MISs 4-2 than during MIS 5, apparently conflicting with the pattern of glacial decrease and interglacial increase in SSTs revealed by previous studies in the SCS [*Wang and Wang*, 1990; *Miao et al.*, 1994; *Wang et al.*, 1995]. Therefore the SSTs here did not systematically vary with glacial-interglacial cycle.

3.3. Reconstruction of the Depth of Thermocline

Numerous tropical ocean studies suggest planktonic foraminiferal species abundance are controlled by upper water temperature and nutrient gradients [*Fairbanks and Wiebe*, 1980; *Fairbanks et al.*, 1982; *Bé et al.*, 1985; *Ravelo et al.*, 1990; *Martinetz*, 1994; *Andreasen and Ravelo*, 1997]. Some researchers have investigated the potential usefulness of very deep dwelling species *G. truncatulinoides* for reconstruction of the upper thermal structure. This species has an unusual life cycle in that it reproduces at ~600 m and from this depth, juveniles rapidly travel to the surface then slowly sink through the water column, growing by adding chambers [*Bé*, 1977; *Bé et al.*, 1985; *Hemleben et al.*, 1989]. For this reason, a higher proportion of this species may indicated a very deep thermocline and/or thick mode water thermostads [*Lohmann and Schweitzer*, 1990; *Lohmann*, 1992; *Ravelo and Fairbanks*, 1992; *Martinez*, 1994, 1997]. The percentage abundance of *G. truncatulinoides* in core 17957-2 (Figure 7) show a trend of gradual decrease during the Brunhes chronozone which indicates the scale of mixing and the DOT have gradually decreased. Especially, *G. truncatulinoides* left-coiling form, which requires a thermocline much deeper than right-coiling form, and *Globoquadrina conglomerata* (lives predominantly below 100 m as adults; [*Bé*, 1977]) abruptly increased in MIS 5 (Figure 7), indicating that the thermal structure of upper water column greatly changed during the time interval.

The average estimated DOT of Holocene (~190 m) agrees with the modern annual DOT derived from the world ocean atlas of *Levitus and Boyer* [1994] in this region. Moreover, the average communality is 0.88, indicating this transfer function technique can interpret 94% of the total variance in the observed faunal information. The estimated DOT ranges from 115 to 230 m in the core, averaging 190 m. Generally, the DOT was relatively deeper during interglacial periods than during glacial periods. The most conspicuous change for the DOT was that it changed little around 200 m before MISs 22-21, that is, before the MPR, and then it gradually decreased during the Brunhes chronozone, with an average of 180 m (Figure 7). The shallowest DOT (~115 m) occurred within MIS 6 and then became deep again after the abrupt increase of *G. truncatulinoides* left-coiling form and *G. conglomerata* in MIS 5.

Previous studies have revealed that when the DOT shoals, the mixed layer-dwelling species (*G. ruber*, *G. sacculifer*, and *Globigerinita glutinata*) decrease, while the thermocline-dwelling species (*P. obliquiloculata*, *G. menardii*, *G. inflata*, and *N. dutertrei*) increase in abundance [*Ravelo et al.*, 1990; *Ravelo and Fairbanks*, 1992]. In core 17957-2 the MPR served as a turning point for the abundances of the mixed layer- and thermocline-dwelling species. The mixed layer-dwelling species decreased in abundance since the MPR and reached minimum during MISs 6-5, while the thermocline-dwelling species changed in an opposite trend (Figure 7), corresponding to the variations of the DOT. In fact, the shallowing of the DOT since the MPR was found also in the western equatorial Pacific [*Schmidt et al.*, 1993].

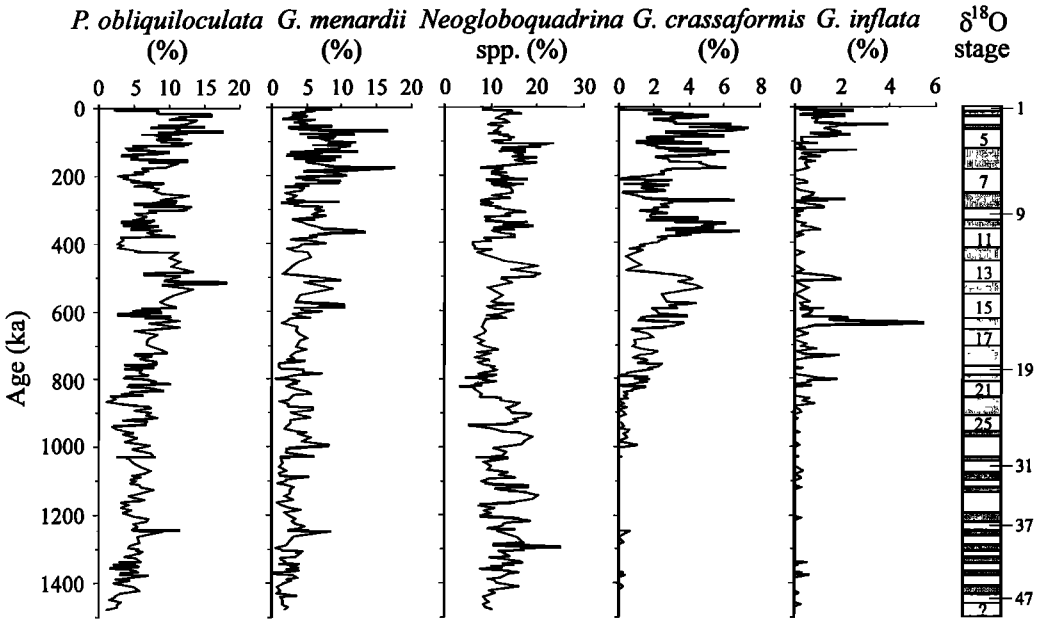

Figure 5. Variations in relative abundance of selected deep-dwelling planktonic foraminiferal species. Marine oxygen isotopic stages are indicated on the right side.

After a minimum shortly before the B/M boundary, the $\delta^{18}O$ difference between *G. sacculifer* and *P. obliquiloculata* continues to increase sharply toward the present at Ocean Drilling Program (ODP) Site 806 on the Ontong Java Plateau. Therefore the tropical DOT in this region has indeed experienced remarkable variations in the Pleistocene.

3.4. Changes of Deep Water Masses

Deep-sea benthic foraminifera has been widely used to reconstruct the late Pleistocene variations in deep water masses, carbonate dissolution, and surface productivity in the SCS for the past few years [*Miao and Thunell*, 1996; *Jian and Wang*, 1997;

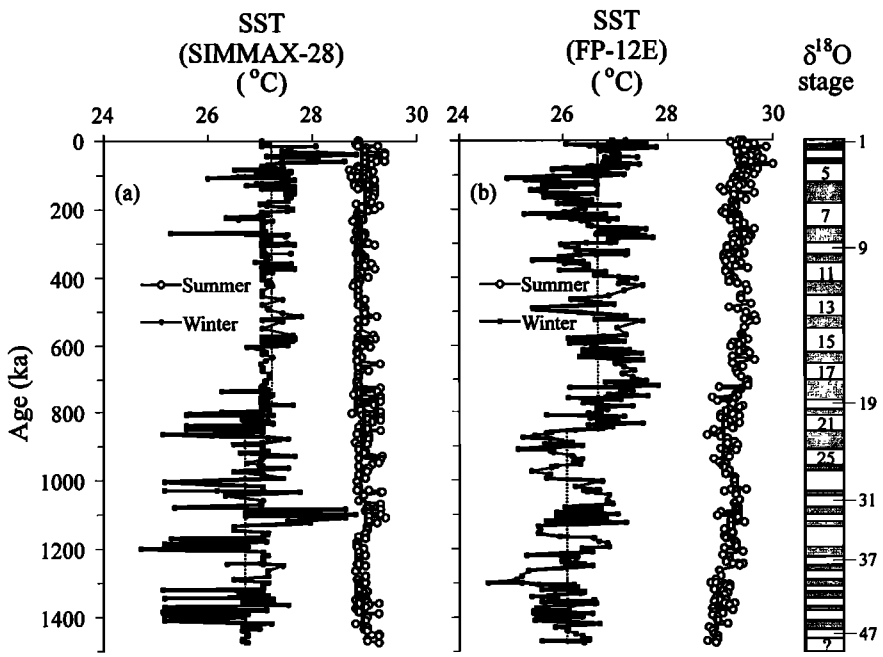

Figure 6. Down-core variations in the (a) SIMMAX-28-derived and (b) FP-12E-derived winter and summer SSTs. Dashed lines show the average winter SST: before and after the B/M boundary (Figure 6a) and before and after MIS 21 (Figure 6b). Marine oxygen isotopic stages are indicated on the right side.

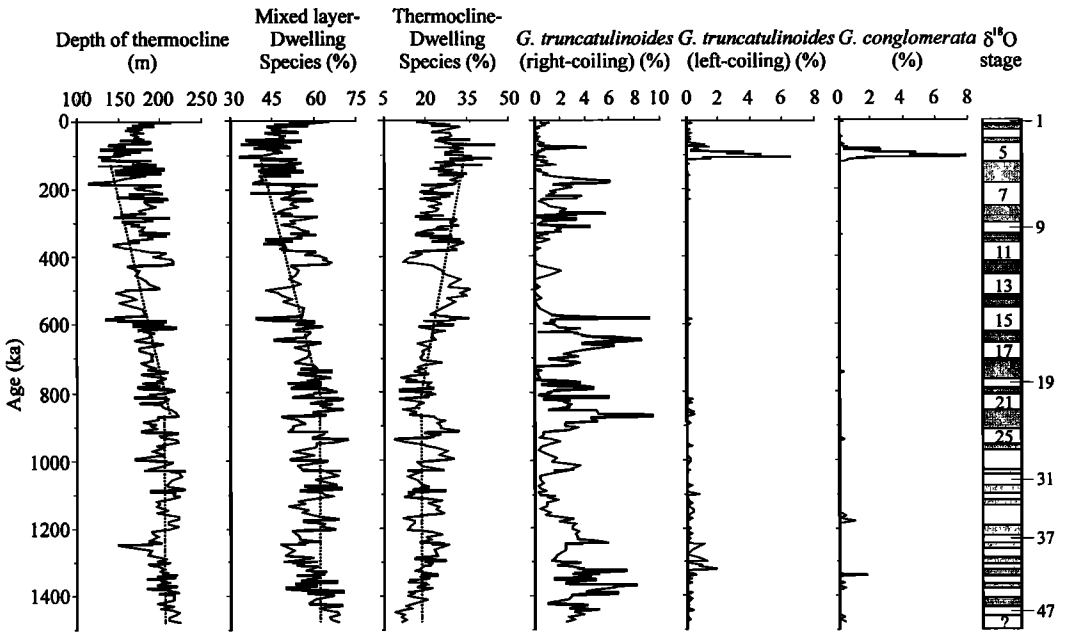

Figure 7. Long-term changes in the DOT estimated using transfer function of *Andreasen and Ravelo* [1997], relative abundances of mixed layer-dwelling species (*Globigerinoides ruber*, *Globigerinoides sacculifer*, and *Globigerinita glutinata*), thermocline-dwelling species (*Pulleniatina obliquiloculata*, *Globorotalia menardii*, *Globorotalia inflata*, and *Neogloboquadrina dutertrei*), right-coiling and left-coiling *Globorotalia truncatulinoides*, and *Globoquadrina conglomerata*. Dashed lines show the general trends of change before and after MISs 22-21. Marine oxygen isotopic stages are indicated on the right side.

Kuhnt et al., 1999]. *Jian et al.* [1999] recently claimed that deep-sea benthic foraminifera in the SCS might be divided into two major groups whose distributions are primarily controlled by the organic flux to the seafloor and the chemical/physical properties in the ambient water mass, respectively. Therefore benthic foraminiferal species and assemblages could be used to monitor the general trend of changes in deep water masses during the Pleistocene in the SCS [*Jian and Wang*, 1997].

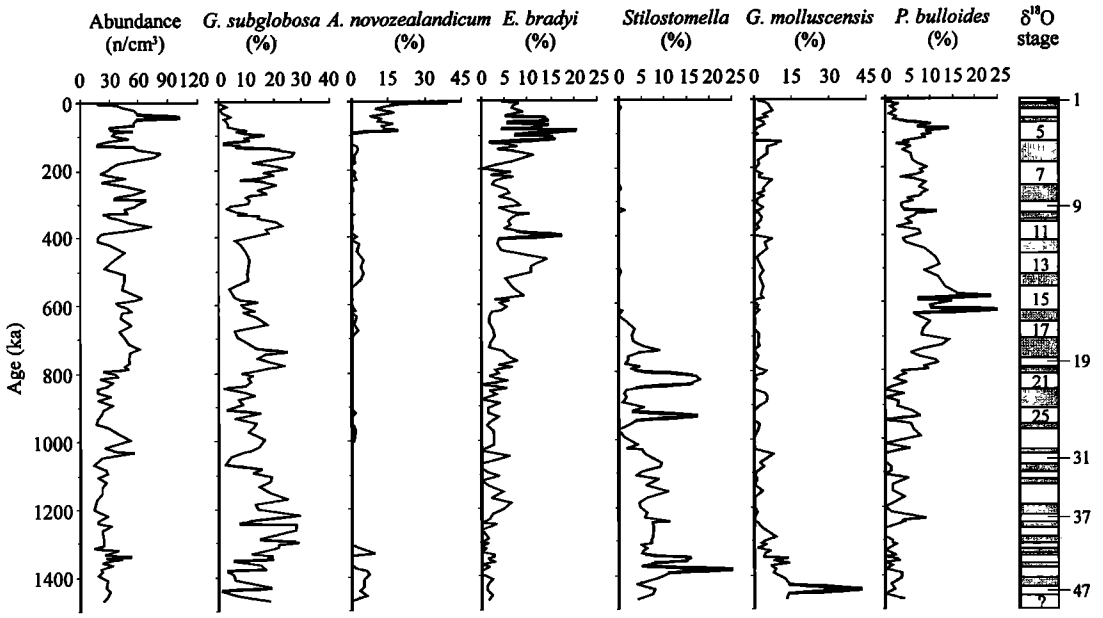

Figure 8. Variations in the abundance of benthic foraminiferal fauna and percentage abundance of main benthic foraminiferal species. Marine oxygen isotopic stages are indicated on the right side.

The abundance of benthic foraminiferal fauna (number of specimens per cubic centimeter) varies between 10 and 110 in the core, with lower values prior to the B/M boundary (Figure 8), implying a great change in deep water conditions at that time. On the basis of the down-core distribution of main benthic foraminiferal species (Figure 8), two important boundaries are found at the B/M boundary and MIS 5. At the B/M boundary, *Pullenia bulloides* increased significantly in abundance, while *Stilostomella* spp. remarkably decreased and then became extinct at the depth of 690 cm. Moreover, since MIS 5, *Globocassidulina subglobosa* obviously decreased in abundance, while *Astrononion novozealandicum* increased. We used *Q* mode factor analysis to better discriminate benthic foraminiferal assemblages. As a result, four varimax factors were obtained, which explain 78.6% of the total variance. According to the down-core variations in factor loadings of each factor (Figure 9) and the factor scores of each species or species groups (Table 3), factor 1, absolutely dominated by *G. subglobosa*, controls most part of the last 1500 kyr before MIS 5. However, factor 2, represented by the *A. novozealandicum* assemblage which is characteristic of *A. novozealandicum* and *Eggerella bradyi* (Figure 8), became more important since MIS 5. Factor 3, dominated by *Stilostomella* spp. and *Globocassidulina molluscensis*, was important before the B/M boundary, especially toward the bottom of the core, while factor 4, represented by the *P. bulloides* assemblage, controlled the period between the B/M boundary and MIS 5.

G. subglobosa is the dominant species of the modern Intermediate Water Mass (IWM) in the SCS as resolved by the same technique [*Jian and Wang*, 1997]. Because factor 1 is characterized by this species, its variations in factor loading should represent the changes of the IWM. From Figure 9 it is inferred that core 17957-2 is bathed in the Deep Water Mass (DWM) now, but it was mainly controlled by the IWM before MIS 5. The remarkable decease in factor 1 and the relative abundance of *G. subglobosa* since MIS 5 indicate that the IWM weakened, as revealed by a previous study [*Jian and Wang*, 1997]. Particularly, the IWM displays a general trend of glacial decrease and interglacial increase, which is obviously superimposed by long-term fluctuations of ~200 kyr.

Compared with those of the IWM, the changes of the DWM are much more complicated. *A. novozealandicum* is the dominant species of the modern DWM in the SCS, especially in the oligotrophic area [*Jian and Wang*, 1997]. The remarkable increase in factor 2 and the relative abundance of this species since MIS 5 indicated that the DWM abruptly strengthened at the expense of the IMW. Before that time, *P. bulloides* assemblage of factor 3 and *Stilostomella* spp. assemblage of factor 4 had successively represented the DWM instead of *A. novozealandicum* assemblage (Figure 9) because *P. bulloides* is one of the characteristic species of the modern DWM [*Jian and Wang*, 1997], while *Stilostomella* spp. is commonly found in cores with present water depths between 1500 and 3000 m [*Schönfeld*, 1996]. The faunal turnovers indicate that there were two major changes in the DWM over the last 1500 kyr. The first one occurred at the B/M boundary, slightly later than the changes in SSTs and DOT. The second one took place within MIS 5, possibly corresponding to the major changes in surface productivity (see Figure 11) and/or the thermal structure of upper water column (Figure 7) at that time.

3.5. Deep-Sea Carbonate Dissolution Fluctuations

The percentage of agglutinated tests in benthic foraminiferal fauna, BF/(BF+PF)%, and relative abundance of agglutinated *E.*

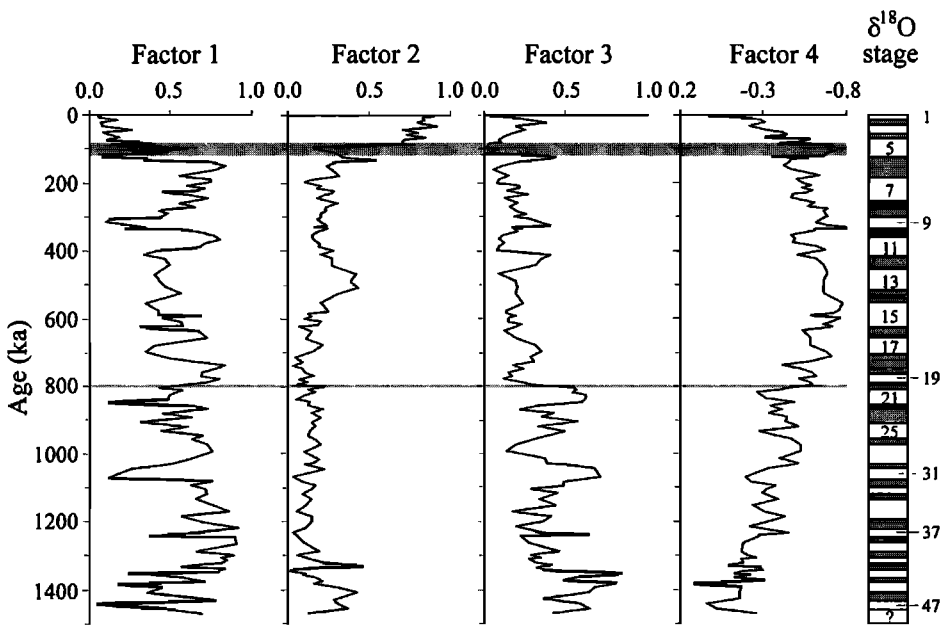

Figure 9. Results of *Q* mode factor analysis on benthic foraminifera, showing down-core variations in factor loading of the four varimax factors. The most important boundaries at the B/M boundary and MIS 5, respectively, are shaded. Marine oxygen isotopic stages are indicated on the right side.

Table 3. Matrix of Factor Scores of the Four Benthic Foraminiferal *Q* mode Varimax Factors

Species / Species Groups	Factor 1	Factor 2	Factor 3	Factor 4
Eggerella bradyi	-0.089	0.314	-0.087	-0.386
Sigmoilopsis schlumbergeri	0.010	-0.008	0.031	-0.002
Pyrgo spp.	-0.009	-0.011	0.218	-0.077
Triloculina tricarinata	-0.020	-0.012	0.198	-0.042
Quinqueloculina seminula	0.015	0.017	0.218	-0.086
Quinqueloculina venusta	-0.009	-0.008	0.039	-0.034
Quinqueloculina spp.	0.003	0.005	0.054	0.006
Lagena spp.	0.020	0.044	0.115	-0.042
Fissurina spp.	0.092	0.109	0.279	-0.203
Nodosaria spp.	0.012	-0.002	0.047	0.013
Dentalina spp.	0.050	0.022	0.131	0.042
Stilostomella spp.	0.087	-0.113	0.639	0.186
Guttulina spp.	0.006	0.039	0.020	-0.037
Bolivina pacific	-0.024	-0.020	0.074	-0.027
Pleurostomella alternans	0.051	-0.012	0.102	0.044
Bulimina alazanensis	-0.013	-0.030	-0.041	-0.244
Bulimina aculeata	-0.077	0.016	0.034	-0.144
Uvigerina peregrina	-0.003	-0.004	0.026	-0.099
Uvigerina auberiana	-0.033	0.112	0.057	-0.050
Reussella spinulosa	-0.010	0.043	0.008	0.000
Francesita advena	-0.001	0.026	0.029	-0.020
Ehrenbergina undulata	0.101	0.031	0.052	0.099
Cassidulina crassa	0.002	0.006	0.006	-0.017
Cassidulina laevigata	0.003	0.137	-0.024	-0.029
Rutherfordoides tenuis	-0.019	-0.008	0.154	0.012
Globocassidulina subglobosa	0.961	-0.032	-0.095	-0.098
Globocassidulina molluscensis	0.006	0.255	0.371	0.108
Favocassidulina favus	-0.006	-0.014	0.045	-0.119
Pullenia bulloides	-0.050	-0.056	-0.067	-0.596
Pullenia quinqueloba	-0.055	0.053	0.190	-0.171
Melonis barleeanum	0.049	0.077	0.013	-0.047
Melonis pompilioides	0.056	-0.021	-0.025	-0.075
Astrononion novozealandicum	0.019	0.798	-0.084	0.209
Elphidium spp.	-0.014	0.023	0.016	-0.008
Epistominella exigua	-0.018	-0.031	0.036	-0.095
Sphaeroidina bulloides	-0.004	0.066	0.033	-0.095
Anomalina globulosa	0.007	-0.005	0.051	-0.049
Hoeglundina elegans	-0.009	0.052	0.006	-0.003
Oridosalia umbonatus	0.055	0.132	0.116	-0.184
Gyroidina orbicularis	-0.013	0.031	-0.003	-0.060
Gyroidinoides lamarckiana	0.006	0.091	0.057	-0.262
Osangularia culter	-0.018	-0.007	0.085	-0.048
Cibicidoides robertsonianus	0.106	0.284	0.016	-0.041
Cibicidoides cf. *robertsonianus*	0.000	-0.019	0.064	-0.015
Cibicidoides wuellerstorfi	-0.028	-0.051	0.207	-0.212
Cibicidoides kullenbergi	0.015	-0.017	0.091	-0.008
Cibicides sp.	0.011	-0.016	0.022	-0.017
Cibicides okinawaensis	0.003	-0.010	0.018	-0.010

bradyi can be used to evaluate deep-sea carbonate dissolution [*Bian et al.*, 1992; *Miao and Thunell*, 1996]. Their obvious increases during the Brunhes chronozone show strengthened dissolution (Figures 8 and 10). In fact, planktonic foraminiferal fragmentation is the best indicator for deep-sea carbonate dissolution [*Le and Shackleton*, 1992; *Miao et al.*, 1994], with high values related to enhanced dissolution. In core 17957-2 the fragmentation curve is negatively well correlated with the coarse fraction and carbonate curves (Figure 10). They display a distinct glacial-interglacial pattern since the MPR. The dissolution spikes with high fragmentation and low coarse fraction and carbonate always occurred in the interglacial stage and the transition from interglacial to glacial stage, for example, MISs 5, 6/7, 8/9, 11, 12/13, 14/15, 17, 18/19, and 21. These spikes can be recognized to correspond to the dissolution events of B3, B5, B7, B9, B11, B13, B15, B17, and M1 in the equatorial Pacific, respectively [*Farrell and Prell*, 1989, 1991]. This typical "Pacific-type" carbonate cycle [*Thunell et al.*, 1992; *Wang et al.*, 1995] in the core further confirms that the SCS shared the same carbonate dissolution signals as the tropical Pacific during the Pleistocene [*Farrell and Prell*, 1989, 1991; *Yasuda et al.*, 1993].

However, the glacial-interglacial pattern of fragmentation is superimposed by a long-term oscillation with an irregular cycle length. Maxima in the fragmentation curve are found at the MPR, MISs 13-11 and MIS 5, in agreement with the changes in the percentage of agglutinated benthic foraminifera and BF/(BF+PF)% (Figure 10). This long-term oscillation of carbonate dissolution has been found in the tropical Pacific and Indian Ocean [*Vincent*, 1981; *Bassinot et al.*, 1994]. Among the three periods of enhanced dissolution, the recent one possibly corresponded to the great changes in planktonic and benthic foraminiferal fauna during MISs 6-5 (Figures 4-9). The middle one centered at ~400 ka is known as the "middle Brunhes dissolution event" [*Farrell and Prell*, 1989; *Bassinot et al.*, 1994]. The lower one at the MPR is not the most striking, though with the highest fragmentation which is not supported by other dissolution indices. Compared to those before the MPR, the average values of fragmentation, percentage of agglutinated benthic foraminifera and BF/(BF+PF)% were higher, while that of coarse fraction and carbonate were lower after the MPR (Figure 10). This implies slightly increased carbonate dissolution as a whole after the MPR in the southern SCS.

3.6. Enhanced Surface Productivity Over the Last 200 kyr

Now it is more than apparent that abundance and species composition of benthic foraminifera are primarily controlled by the organic carbon flux to the seafloor and thus, ultimately, by the surface productivity [*Herguera and Berger*, 1991; *Sarnthein and Altenbach*, 1995; *Miao and Thunell*, 1996; *Jian et al.*, 1999; *Kuhnt et al.*, 1999]. It has been found that benthic foraminifera *Bulimina aculeata* and *Uvigerina peregrina* are well associated with high surface productivity in the SCS [*Miao and Thunell*, 1996; *Jian et al.*, 1999]. Their relative abundances are generally <5% in the core (Figure 11), indicating a very low surface productivity at this site, which is consistent with the modern distribution of surface primary productivity in the SCS [*The Multidisciplinary Oceanographic Expedition Team*, 1992]. Nevertheless, the relative abundance of *B. aculeata* and *U. peregrina* generally increased during glacial periods, especially in MISs 22, 8, and 6, indicating that the productivity slightly increased at these times.

Biogenic opal is a parameter related to the surface productivity [*Herguera and Berger*, 1991; *Murray et al.*, 1993]. The percentage of opal in the core ranges from 2.7 to 28.3%, with an important boundary at ~200 ka around MISs 6/7. The average value of opal content before 200 ka is only 6.6%, while that of the last 200 kyr is as high as 15.7% (Figure 11). This enhanced surface productivity over the last 200 kyr is also confirmed by the obviously decreased abundance of *Cibicidoides wuellerstorfi* (Figure 11), an epifaunal species often associated with low surface productivity [*Sarnthein and Altenbach*, 1995; *Miao and Thunell*, 1996; *Jian et al.*, 1999].

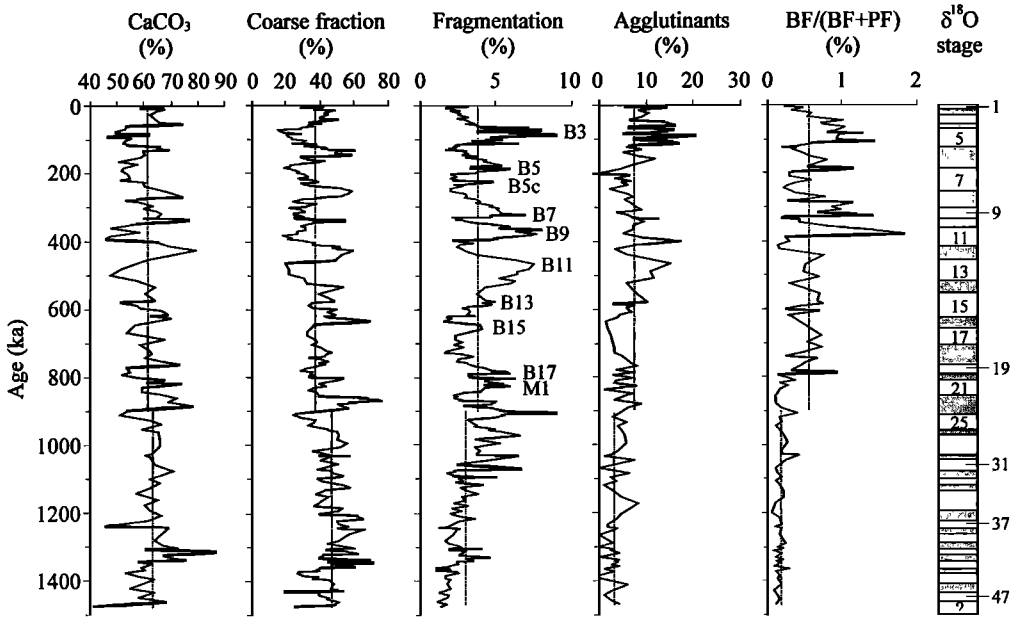

Figure 10. Deep-sea carbonate dissolution indices versus depth. B3~17 and M1 indicate major spikes of the fragmentation curve according to their corresponding dissolution events in the equatorial Pacific [*Farrell and Prell*, 1989, 1991]. Dashed lines show the average values before and after the MPR, respectively. Marine oxygen isotopic stages are indicated on the right side.

3.7. Periodic Variations in Paleoceanographic Records

Spectral analysis was used to study the variability of four paleoceanographic records ($\delta^{18}O$, *G. truncatulinoides* percent, FP-12E-derived winter SST, and IWM) for the last 1500 kyr (Figure 12). The IMW is represented by the factor loadings of benthic foraminiferal factor 1 as above discussed. After SPECTRUM has performed the analysis, some statistical parameters are displayed. Probably the most important is the reliable frequency range. Assuming that at least two full cycles are observed within each WOSA segment, the lowest reliable frequency in this study is 0.0027 1/kyr, corresponding to the period of 370 kyr. The spectral peaks with lower frequency than this limit are discarded in the study.

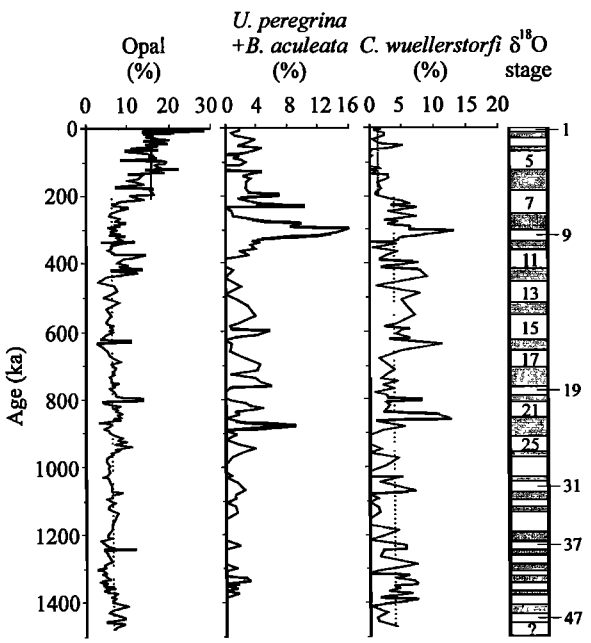

Figure 11. Down-core variations in the surface paleoproductivity indices. Dashed lines show the average values before and after 200 ka, respectively. Marine oxygen isotopic stages are indicated on the right side.

According to Figure 12a, the $\delta^{18}O$ record reveals clear eccentricity-dominated (~100 kyr) and processional (~23 kyr) signals but with weak obliquity-related (~41 kyr) response as expected. However, the obliquity response became more important for the early Pleistocene, corresponding to the climatic transformation at the MPR [*Berger et al.*, 1993a] which has been also found by previous studies on Chinese loess [*Liu and Ding*, 1993; *Ding et al.*, 1994]. An outstanding result of the spectral analyses is the existence of long-term oscillations of ~200 kyr for the records of upper water structure (e.g., *G. truncatulinoides* percent and winter SST) and deep water conditions (e.g., the IWM), with weak ~100 kyr eccentricity-related responses (Figures 12c and 12d). The obliquity-related (~46 kyr) responses for the records of upper water structure are more significant than that for the IWM record, in contrast to the spectrum of the $\delta^{18}O$ record. The ~200-kyr cyclicity has already been revealed in the *G. truncatulinoides* percent by previous study in the equatorial western Pacific [*Martinez*, 1994, 1997]. It is not confined to the upper water column but also occurred in the deep water of the SCS as shown by this study. We are not sure if the ~200-kyr cyclicity is a real cycle or not for the changes of the upper water structure and deep water conditions, and if so, its dynamics are still not clear. We suggest it possibly represents the second harmonic of the ~400 kyr period of eccentricity which became more important before the late Pleistocene ice age regime [*Clemens and Tiedemann*, 1997]. Therefore our data support eccentricity's role in the origin of low-frequency paleoceanographic oscillations in three dimensions of the WPWP.

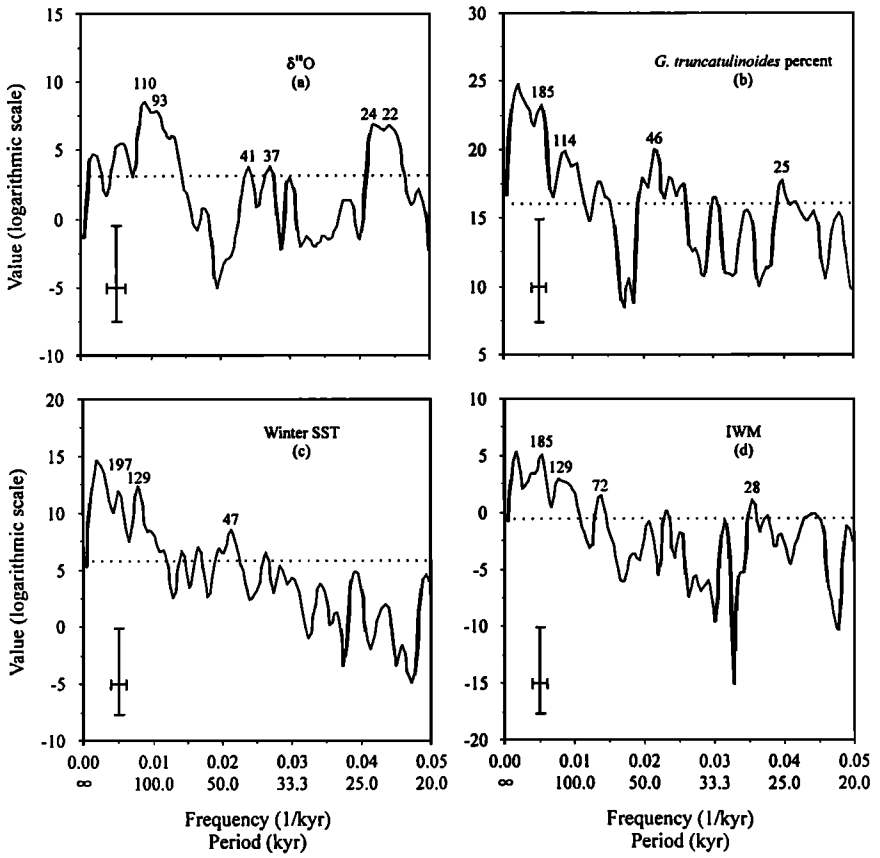

Figure 12. Spectral analysis of four paleoceanographic records: (a) $\delta^{18}O$, (b) *Globorotalia truncatulinoides* percent, (c) winter SST estimated using FP-12E transfer function, and (d) IWM for the last 1500 kyr (Settings: OFAC = 4.0; HIFAC = 1.0; number of segments is three; Welch window except Hanning window for $\delta^{18}O$. See *Schulz and Stattegger* [1997] for detailed description of these parameters). Numbers above peaks denote respective periods. Cross in lower left corner marks 6-dB bandwidth (horizontal) and 80% confidence interval (vertical). Horizontal dashed line denotes the average value of the spectrum and is a rough estimate for a white noise component in the time series. Considering only those parts of spectral peaks above this level gives an estimation of their corresponding variance contribution.

4. Discussion

Variations of the SSTs and DOT in the SCS are primarily a response to monsoonal wind-driven surface circulation [*Wyrtki*, 1961]. Core 17957-2 is located in the tropical SCS, where the foraminifera-based paleo-SST reconstruction has been a vigorous point of discussion in recent years [*Pflaumann and Jian*, 1999]. In this study, we applied two different transfer functions SIMMAX-28 and FP-12E. Both results show that the SSTs here have no consistent glacial-interglacial changes. Though there is nearly no tendency of point-by-point comparable SSTs, both results reveal (1) the slightly increased SSTs as a whole right after MISs 22-20 and (2) the obviously decreased winter SST during MISs 6-5.

Comparatively speaking, we have little knowledge about the variation of modern DOT in the SCS. Being a part of the WPWP, the southern SCS has other effects on its variation in the DOT except the East Asian monsoonal wind system. For example, the variations in the magnitude of the trade winds and associated equatorial currents may affect regional SCS circulation [*Wyrtki*, 1961]. Especially, during the Pleistocene glacial periods the SCS changed its configuration into a semienclosed basin due to the exposed shelf [*Wang et al.*, 1995]. This caused the outflow of subsurface water from the SCS into the Indian Ocean [*Wyrtki*, 1961] to be unlikely and altered the upper water structure of the southern SCS. The DOT there indeed experienced significant variations over the last 1500 kyr. Since the MPR, the DOT gradually became shallower until MISs 6-5 and then deepened afterward, as also confirmed by the changes in very deep dwelling species *G. truncatulinoides*. The shallowest DOT in MIS 6 can be used to evoke an upwelling enhancing the surface productivity.

It is interesting that the two major changes in deep water masses of the southern SCS were almost synchronous with those in surface water masses but generally with a potential lag in response. For example, planktonic foraminiferal fauna responded to the MPR immediately, while benthic foraminiferal fauna did not change until the B/M boundary. As for the paleoceanographic changes within MISs 6-5, the winter SSTs, DOT, and surface productivity greatly changed since MIS 6, while the deep water masses changed since MIS 5. Therefore both the surface and deep circulation in the southern SCS had experienced significant variations over the last 1500 kyr.

A variety of interpretations have been suggested to explain the striking paleoceanographic changes at the MPR, such as changes in North Atlantic Deep Water production [*Farrell and Prell*, 1991], increase of marine-based ice sheets, uplift of highlands from erosion, and tectonic forces [*Ruddiman and Raymo*, 1988; *Berger*

et al., 1993b]. The great changes within MISs 6-5, however, are addressed for the first time in the deep-sea areas of the western Pacific. The present study has no intention of drawing any conclusion on the nature of the two major Pleistocene paleoceanographic changes at the MPR and MISs 6-5 but only proposes possible links between paleoceanography and tectonics to interpret why the planktonic and benthic foraminiferal records show great changes at these times.

Despite the considerable dispute about timing and mechanism of the uplift of the Tibetan Plateau it is generally believed that the uplift has played a key role in adjusting Asian and Northern Hemispheric atmospheric circulation [*Kutzbach et al.*, 1989; *Molnar and England*, 1990; *Li*, 1991; *Harrison et al.*, 1991]. On the basis of the geological records of Tibetan Plateau and adjacent regions the uplift of the Plateau intensified since 3.6 Ma with three successive stages: 3.6-1.7 Ma, 1.1-0.6 Ma, and around 0.15 Ma [*Li*, 1991; *Li and Fang*, 1998]. The tectonic episode around 0.8 Ma was the most remarkable within the second stage when the plateau was uplifted to 3000-3500 m and entered into the cryosphere [*Shi and Zheng*, 1996; *Li and Fang*, 1998]. This episode coincided with the climatic transformation at the MPR revealed in the Chinese loess [*Liu and Ding*, 1993; *Ding et al.*, 1994] and deep-sea sediments in the western equatorial Pacific [*Berger et al.*, 1993a] and the SCS (see above). The tectonic event around 0.15 Ma resulted in the cutting through of the Long Yang Gorge [*Li*, 1991], which eventually brought about the entire Yellow River flowing eastward into the sea [*Wu et al.*, 1998]. This tremendous geomorphological change coincided with the onset of the extensive late Pleistocene marine transgression in East China [*Wang et al.*, 1985; *Yang et al.*, 1996], suggesting that the China offshore subsided at that time. Because the accelerating uplift of Tibetan Plateau has been suggested to be responsible for both the late Cenozoic global cooling and the intensification of Asian monsoon [e.g., *Ruddiman and Kutzbach*, 1989], we speculated it might be the tectonic events in China around 1.1-0.6 Ma and 0.15 Ma that caused important evolutionary changes in the East Asian monsoon. These major changes, furthermore, led to the reorganization of surface and deep circulation in the SCS, which were reflected by a series of paleoceanographic changes recorded in planktonic and benthic foraminifera.

However, the relationships between tectonics, climate, and paleoceanography are complex and highly nonlinear. It is likely that the middle and late Pleistocene major paleoceanographic changes in the SCS shall remain a mystery yet for some time, and the questions regarding their natures require a broad attack using many different signals from various environments [*Imbrie et al.*, 1989; *Berger et al.*, 1993a]. Fortunately, for possible further work on it, ~5500 m sediment from the northern and southern slopes of the SCS, which have been recovered by JOIDES Resolution in 1999 during ODP Leg 184 [*Prell et al.*, 1998], can be studied. We believe it will make a substantial contribution to understanding links between uplift of the Tibetan Plateau and major Pleistocene paleoceanographic changes in the SCS.

5. Conclusions

1. Core 17957-2 from the southern SCS provides nearly continuous paleoceanographic records of the last 1500 kyr on the basis of $\delta^{18}O$ curve of *G. sacculifer* and coarse fraction stratigraphy, as well as magnetostratigraphy and microfossil (including planktonic and benthic foraminifera, nannofossil, and radiolarian) biostratigraphy. Two major Pleistocene paleoceanographic changes were found: One was the MPR at the entrance of MIS 22 (near 900 ka); the other occurred within MISs 6-5 (centered at 130 ka).

2. Using planktonic foraminiferal transfer functions, we found that the SST rose, while the DOT shoaled after the MPR in the southern SCS. Since the MPR, the DOT gradually became shallower until MISs 6-5 and then deepened afterward, as confirmed by the changes in very deep dwelling species *G. truncatulinoides*. Particularly, the relative abundance of *G. truncatulinoides* left-coiling form and *G. conglomerata* abruptly increased within MIS 5 while the winter SSTs obviously decreased.

3. The IWM and carbonate dissolution display a pattern of glacial decrease and interglacial increase. The dissolution spikes in the southern SCS can be well correlated with the dissolution events in the equatorial Pacific, indicating that the SCS shares the same carbonate dissolution signals as the tropical Pacific. There were two major changes in the DWM, at the B/M boundary and MIS 5 respectively, reflected by three successive deep-sea benthic foraminiferal assemblages. Judging from the results of benthic foraminiferal factor analysis and down-core distributions of characteristic species, the influence of the DWM gradually increased during the Brunhes chronozone and remarkably strengthened since MIS 5, while that of the IWM decreased at the same time. In addition, the variations in the biogenic opal content and relative abundance of *Uvigerina* plus *Bulimina* and *C. wuellerstorfi* reveal that the surface productivity was greatly enhanced over the last 200 kyr.

4. Generally, benthic foraminifera lagged behind planktonic foraminifera in their response to the two major Pleistocene paleoceanographic changes. For example, planktonic foraminiferal fauna responded to the MPR immediately, while benthic foraminiferal fauna did not changed until the Brunhes/Matuyama boundary. As for the major paleoceanographic changes within MISs 6-5, the winter SSTs, DOT, and surface paleoproductivity greatly changed since MIS 6 (near 200 ka), while the deep water masses changed since MIS 5. We speculated that the two major Pleistocene paleoceanographic changes might be related to the reorganization of surface and deep circulation in the SCS possibly induced by tectonic forces (e.g., the intensified uplift of Tibetan Plateau).

5. The oxygen isotope record for ice mass fluctuations has clear ~100 kyr eccentricity-dominated signals after the MPR, but with significant precession- and obliquity-related response before the MPR. The upper water structure (e.g., SST and *G. truncatulinoides* percent) and deep water conditions (e.g., the IWM) display long-term oscillations of ~200 kyr (perhaps representing the second harmonic of the ~400 kyr period of eccentricity) for the last 1500 kyr. Our data support eccentricity's role in the origin of low-frequency paleoceanographic oscillations in three dimensions of the WPWP.

Acknowledgements. We would like to thank the crew and scientists aboard the *R/V SONNE* for assistance during Cruise 95; M. Sarnthein and S. Clemens for helpful discussion; D. Budziak for help in the spectral analysis; and W. Huang for assistance in preparation of the manuscript. T. Barrows and D. Andreasen reviewed the manuscript and their comments, suggestions, and constructive criticisms greatly improved the manuscript. This work was funded by the National Natural Science Foundation of China (grants 49999560 and 49776290), the Trans-Century Training Program Foundation for the Talents by the Ministry of Education of China, and the Alexander von Humboldt Foundation of Germany.

References

Andreasen, D. J., and A. C. Ravelo, Tropical Pacific Ocean thermocline depth reconstructions for the Last Glacial Maximum, *Paleoceanography, 12(3)*, 395-413, 1997.

Andree, M., et al., AMS radiocarbon dates on foraminifera from deep sea sediments, *Radiocarbon, 28(2A)*, 424-428, 1986.

Barker, R. W., Taxonomic notes on the species figured by H.B. Brady in his report on the foraminifera dredged by H.M.S. "Challenger" during the years 1873-1876, *Spec. Publ. Soc. Econ. Paleontol. Mineral., 9*, 1-238, 1960.

Bassinot, F. C., L. Beaufort, E. Vincent, L. D. Labeyrie, F. Rostek, P. J. Müller, X. Quideleur, and Y. Lancelot, Coarse fraction fluctuations in pelagic carbonate sediments from the tropical Indian Ocean: A 1500-kyr record of carbonate dissolution, *Paleoceanography, 9(4)*, 579-600, 1994.

Bé, A. W. H., An ecological, zoogeographic and taxonomic review of recent planktonic foraminifera, in *Oceanic Micropaleontology, vol. 1*, edited by A. T. S. Ramsay, pp. 1-100, Academic, San Diego, Calif., 1977.

Bé, A. W. H., J. K. B. Bishop, M. S. Sverdlove, and W. D. Gardner, Standing stock, vertical distribution and flux of planktonic foraminifera in the Panama Basin, *Mar. Micropaleontol., 9*, 307-333, 1985.

Berger, W. H., Ocean ventilation during the last 12,000 years: Hypothesis of counterpoint deep water production, *Mar. Geol., 78*, 1-10, 1987.

Berger, W. H., T. Bickert, H. Schmidt, and G. Wefer, Quaternary oxygen isotope record of pelagic foraminifers: Site 806, Ontong Java Plateau, *Proc. Ocean Drill. Program Sci. Results, 130*, 381-396, 1993a.

Berger, W. H., T. Bickert, E. Jansen, G. Wefer, and M. Yasuda, The central mystery of the Quaternary ice age, *Oceanus, 36(4)*, 53-56, 1993b.

Berggren, W. A., D. V. Kent, C. C. Swisher III, and M. P. Aubry, A Revised Cenozoic geochronology and chronostratigraphy, in *Geochronology, Time Scales and Global Stratigraphic Correlation*, edited by W. A. Berggren, et al., *Spec. Publ. Soc. Econ. Paleontol. Mineral., 54*, 129-212, 1995.

Bian, Y., P. Wang, and L. Zheng, Deep-water dissolution cycles of late Quaternary planktonic foraminifera in the South China Sea (in Chinese, with English abstract), in *Contributions to Late Quaternary Paleoceanography of the South China Sea*, edited by Z. Ye and P. Wang, pp. 261-273, Qingdao Ocean Uni. Press, Qingdao, China, 1992.

Broecker, W. S., M. Andree, M. Klass, G. Bonani, W. Wolfli, and H. Oeschger, New evidence from the South China Sea for an abrupt termination of the last glacial period, *Nature, 333*, 156-158, 1988.

Chen, M.-T., H.-W. Ho, T.-D. Lai, L. Zheng, Q. Miao, K.-S. Shea, M.-P. Chen, P. Wang, K.-Y. Wei, and C.-Y. Huang, Recent planktonic foraminifers and their relationships to surface ocean hydrography of the South China Sea, *Mar. Geol., 146*, 173-190, 1998.

Clemens, S., and R. Tiedemann, Eccentricity forcing of Pliocene-Early Pleistocene climate revealed in a marine oxygen-isotope record, *Nature, 385*, 801-804, 1997.

Climate: Long-Range Investigation, Mapping, and Prediction (CLIMAP) Project Members, Seasonal reconstructions of the Earth's surface at the last glacial maximum, *Geol. Soc. Am. Map Chart Ser., MC-36*, 1-18, 1981.

Ding, Z. L., Z. W. Yu, N. W. Rutter, and T. S. Liu, Towards an orbital time scale for Chinese loess deposits, *Quat. Sci. Rev., 13*, 39-70, 1994.

Fairbanks, R. G., and P. H. Wiebe, Foraminifera and chlorophyll maximum: Vertical distribution, seasonal succession, and paleoceanographic significance, *Science, 209*, 1524-1526, 1980.

Fairbanks, R. G., M. Sverdlove, R. Free, P. H. Wiebe, and A. W. H. Bé, Vertical distribution and isotopic fractionation of living planktonic foraminifera from the Panama Basin, *Nature, 298*, 841-844, 1982.

Farrell, J. W., and W. Prell, Climate change and $CaCO_3$ preservation: An 800,000 year bathymetric reconstruction from the central equatorial Pacific Ocean, *Paleoceanography, 4*, 447-466, 1989.

Farrell, J. W., and W. Prell, Pacific $CaCO_3$ preservation and $\delta^{18}O$ since 4 Ma: Paleoceanographic and paleoclimatic implications, *Paleoceanography, 6*, 485-498, 1991.

Glass, B., Microtektites in deep-sea sediments, *Nature, 214*, 373-374, 1967.

Harrison, T. M., P. Copeland, W. S. F. Kidd, and A. Yin, Raising Tibet, *Science, 255*, 1663-1670, 1991.

Herguera, J. C., and W. Berger, Paleoproductivity from benthic foraminifera abundance: Glacial to postglacial change in the west-equatorial Pacific, *Geology, 19*, 1173-1176, 1991.

Hemleben, G., M. Splinder, and O. R. Anderson, *Modern Planktonic Foraminifera*, 363 pp., Springer-Verlag, New York, 1989.

Imbrie, J., A. McIntyre, and A. Mix, Oceanic response to orbital forcing in the late Quaternary: Observational and experimental strategies, in *Climate and Geo-Sciences*, edited by A. Berger, S. Schneider, and J. C. Duplessy, pp. 121-164, Kluwer Acad., Norwell, Mass., 1989.

Jian, Z., and L. Wang, Late Quaternary benthic foraminifera and deep-water paleoceanography in the South China Sea, *Mar. Micropaleontol., 32*, 127-154, 1997.

Jian, Z., L. Wang, M. Kienast, M. Sarnthein, W. Kuhnt, H.-L. Lin, and P. Wang, Benthic foraminiferal paleoceanography of the South China Sea over the last 40,000 years, *Mar. Geol., 156(1-4)*, 159-186, 1999.

Kennett, J. P., and M. S. Srinivasan, *Neogene Planktonic Foraminifera, A Phylogenetic Atlas*, 265 pp., Hutchinson Ross, Stroudsburg, 1983.

Klovan, J. E., and J. Imbrie, An algorithm and FORTRAN IV program for large scale Q-mode factor analysis, *J. Int. Assoc. Math. Geol., 3*, 61-78, 1971.

Kuhnt, W., S. Hess, and Z. Jian, Quantitative composition of benthic foraminiferal assemblages as a proxy indicator for organic carbon flux rates in the South China Sea, *Mar. Geol., 156(1-4)*, 123-157, 1999.

Kukla, G. J., and Z. An, Loess stratigraphy in central China, *Palaeogeogr. Palaeoclimatol. Palaeoecol., 72*, 203-225, 1989.

Kutzbach, J. E., P. J. Guetter, W. F. Ruddiman, and W. L. Prell, Sensitivity of climate to late Cenozoic uplift in Southern Asia and the American West: Numerical experiments, *J. Geophys. Res., 94(D15)*, 18,393-18,407, 1989.

Le, J., and N. J. Shackleton, Carbonate dissolution fluctuations in the western equatorial Pacific during the late Quaternary, *Paleoceanography, 7(1)*, 21-42, 1992.

Levitus, S., and T. P. Boyer, *World Ocean Atlas 1994, vol. 4, Temperature, NOAA Atlas NESDIS 4*, 117 pp., Nati. Oceanic and Atmos. Admin., Silver Spring, Ma., 1994.

Li, B., Paleoceanography of the Nansha Area, southern South China Sea since the last 700,000 years (in Chinese, with English abstract), Ph.D. thesis, 96 pp., Nanjing Inst. of Geol. and Paleontol., Acad. Sinica, Nanjing, China, 1997.

Li, J., The environmental effects of the uplift of the Qinghai-Xizang Plateau, *Quat. Sci. Rev., 10*, 479-483, 1991.

Li, J., and X. Fang, Studies on the uplift and environmental change of the Qinghai-Xizang Plateau (in Chinese), *Chin. Sci. Bull., 43(15)*, 1569-1574, 1998.

Liu, T., and Z. Ding, Stepwise coupling of monsoon circulations to global ice volume variations during the late Cenozoic, *Global Planet. Change, 7(1-3)*, 119-130, 1993.

Loeblich, A. R., Jr., and H. Tappan, *Foraminiferal Genera and Their Classification*, 868 pp., Van Nostrand Reihhold, New York, 1988.

Lohmann, G. P., Increasing seasonal upwelling in the subtropical South Atlantic over the past 700,000 yrs: Evidence from deep-living planktonic foraminifera, *Mar. Micropaleontol., 19*, 1-12, 1992.

Lohmann, G. P., and P. N. Schweitzer, *Globorotalia truncatulinoides* growth and chemistry as probes of the past thermocline, 1, Shell size, *Paleoceanography, 5(1)*, 55-75, 1990.

Martinez, J. I., Late Pleistocene paleoceanography of the Tasman Sea: Implications for the dynamics of the warm pool in the western Pacific, *Palaeogeogr. Palaeoclimatol. Palaeoecol., 112*, 19-62, 1994.

Martinez, J. I., Decreasing influence of Subantarctic Mode Water north of the Tasman Front over the past 150 kyr, *Palaeogeogr Palaeoclimatol. Palaeoecol., 131*, 355-364, 1997.

Miao, Q., and R. C. Thunell, Late Pleistocene-Holocene distribution of deep-sea benthic foraminifera in the South China Sea and Sulu Sea: Paleoceanographic implications, *J. Foraminiferal Res. 26(1)*, 9-23, 1996.

Miao, Q., R. C. Thunell, and D. M. Anderson, Glacial-Holocene paleoceanography of the western equatorial Pacific Ocean: Carbonate dissolution and sea surface temperature in the South China and Sulu Seas, *Paleoceanography, 9(1)*, 69-90, 1994.

Molnar, P., and P. England, Late Cenozoic uplift of mountain ranges and global climate change: Chicken or egg?, *Nature, 346*, 29-34, 1990.

Molnia, B. F., A rapid and accurate method for the analysis of calcium carbonate in small samples, *J. Sediment. Petrol., 44*, 589-590, 1974.

Moore, T. C., Radiolarian stratigraphy, Leg 138, *Proc. Ocean Drill. Program Sci. Results, 138*, 191-232, 1995.

Mortlock, R. A., and P. N. Froelich, A simple method for the rapid determination of biogenic opal in pelagic marine sediments, *Deep Sea Res., Part A, 36*, 1415-1426, 1989.

Murray, D. W., J. W. Farrell, and V. Mckenna, Biogenic sedimentation at Site 847, eastern equatorial Pacific Ocean during the past 3 m.y., *Proc. Ocean Drill. Program Sci. Results, 138*, 429-460, 1993.

Parker, F. L., Planktonic foraminiferal species in Pacific sediments, *Micropaleontology, 8*, 219-254, 1962.

Pflaumann, W., and Z. Jian, Modern distribution patterns of planktonic foraminifera in the South China Sea and west Pacific: A new transfer

technique to estimate regional sea-surface temperatures, *Mar. Geol., 156(1-4)*, 41-83, 1999.

Prell, W., P. Wang, and P. Blum, Ocean Drilling Program Leg 184 scientific prospectus, *Ocean Drill. Program Sci. Prospectus, 83*, 1-71, 1998.

Ravelo, A. C., and R. G. Fairbanks, Oxygen isotopic composition of multiple species of planktonic foraminifera: Recorders of the modern photic zone temperature gradient, *Paleoceanography, 7(6)*, 815-831, 1992.

Ravelo, A. C., R. G. Fairbanks, and S. G. H. Philander, Reconstructing tropical Atlantic hydrography using planktonic foraminifera and an ocean model, *Paleoceanography*, 5(3), 409-431, 1990.

Ruddiman, W. F., and J. E. Kutzbach, Forcing of Late Cenozoic Northern Hemisphere climate by plateau uplift in Southern Asia and the American West, *J. Geophys. Res., 94*, 18,409-18,427, 1989.

Ruddiman, W. F., and M. E. Raymo, Northern Hemisphere climatic regimes during the past 3 Ma: Possible tectonic connections, *Philos. Trans. R. Soc. London, Ser. B, 318*, 411-430, 1988.

Ruddiman, W. F., M. E. Raymo, D. G. Martinson, B. M. Clement, and J. Backman, Pleistocene evolution: Northern Hemisphere ice sheets and North Atlantic Ocean, *Paleoceanography, 4*, 353-412, 1989.

Sarnthein, M., and A. V. Altenbach, Late Quaternary changes in surface water and deep water masses of the Nordic Seas and north-eastern North Atlantic: A review, *Geol. Rundsch, 84*, 89-107, 1995.

Sarnthein, M., U. Pflaumann, P. Wang, and H.-K. Wong (Eds.), *Preliminary Report on Sonne-95 Cruise "Monitor Monsoon" to the South China Sea, Ber. Rep. 68*, 225 pp., Geol.-Paläont. Inst. Univ. Kiel, Kiel, Germany, 1994.

Schmidt, H., W. H. Berger, T. Bickert, and G. Wefer, Quaternary carbon isotope record of pelagic foraminifers: Site 806, Ontong Java Plateau, *Proc. Ocean Drill. Program Sci. Results, 130*, 397-409, 1993.

Schönfeld, J., The "Stilostomella Extinction", Structure and dynamics of the last turnover in deep-sea benthic foraminiferal assemblages, in *Microfossils and Oceanic Environments*, edited by A. Mogurlevsky and R. Whatly, pp. 27-37, Uni. of Wales, Aberystwth Press, Aberystwth, 1996.

Schulz, M., and K. Stattegger, Spectrum: Spectral analysis of unevenly spaced paleoclimatic time series, *Comput. Geosci., 23(9)*, 929-945, 1997.

Shackleton, N. J., A. Berger, and W. R. Peltier, An alternative astronomical calibration of the lower Pleistocene time scale based on ODP Site 677, *Trans. R. Soc. Edinburgh Earth Sci., 81*, 251-261, 1990.

Shackleton, N. J., J. G. Baldauf, J.-A. Flores, M. Iwai, T. C. Moore Jr., I. Raffi, and E. Vincent, Biostratigraphic summary for Leg 138, *Proc. Ocean Drill. Program Sci. Results, 138*, 517-536, 1995.

Shi, Y., and B. Zheng, Timing and height of the Qinghai-Xizang Plateau uplifting into the cryosphere and its impact on the surrounding area (in Chinese), in *Formation, Environmental Evolution and Ecological System of Tibetan Plateau, Annuals (1995)*, edited by Qingzang Programme Comm., pp. 136-146, Sci. Press, Beijing, 1996.

Smit, J, A. J. M. van Eijden, and S. R. Troelstra, Analysis of the Australasian microtektite event, the Toba Lake event, and the Cretaceous/Paleogene boundary, eastern Indian Ocean, *Proc. Ocean Drill. Program Sci. Results, 121*, 489-503, 1991.

Sun, X., and X. Li, A pollen record of the last 37 ka in deep sea core 17940 from the northern slope of the South China Sea, *Mar. Geol., 156(1-4)*, 227-244, 1999.

Tauxe, L., J. L. LaBreque, R. Dodson, M. Fuller, and J. Dematteo, "U"-channel – A new technique for paleomagnetic analysis of hydraulic piston cores, *Eos Trans. AGU, 64 (18)*, 219, 1983.

The Multidisciplinary Oceanographic Expedition Team of Chinese Academy of Sciences to the Nansha Islands, *Quaternary Coral Reef Geology of Yongshu Reef, Nansha Islands* (in Chinese, with English abstract), 264 pp., China Ocean Press, Beijing, 1992.

Thierstein, H. R., K. R. Geitzenauer, B. Molfino, and N. J. Shackleton, Global synchroneity of late Quaternary coccolith datum levels: Validation by oxygen isotopes, *Geology, 5*, 400-404, 1977.

Thompson, P. R., Planktonic foraminifera in the western North Pacific during the past 150,000 years: Comparison of modern and fossil assemblages, *Palaeogeogr. Palaeoclimatol. Palaeoecol., 35*, 241-279, 1981.

Thompson, P. R., A. W. H. Bé, J.-C. Duplessy, and N. J. Shackleton, Disappearance of pink-pigmented *Globigerinoides ruber* at 120,000 yr B.P. in the Indian and Pacific Oceans, *Nature, 280*, 554-558, 1979.

Thunell, R. C., Q. Miao, S. E. Calvert, and T. F. Pedersen, Glacial-Holocene biogenic sedimentation patterns in the South China Sea: Productivity variations and surface water pCO_2, *Paleoceanography, 7(2)*, 143-162, 1992.

Thunell, R. C., D. Anderson, D. Gellar, and Q. Miao, Sea-surface temperature estimates for the tropical Western Pacific during the last glaciation and their implications for the Pacific Warm Pool, *Quat. Res., 41*, 255-264, 1994.

Vincent, E., Carbonate stratigraphy of Hess Rise, Central North Pacific and paleoceanographic implications, *Initial Rep. Deep Sea Drill. Proj., 62*, 571-606, 1981.

Wang, L., Sea surface temperature history of the low latitude western Pacific during the last 5.3 million years, *Palaeogeogr. Palaeoclimatol. Palaeoecol., 108(3/4)*, 379-436, 1994.

Wang, L., and P. Wang, Late Quaternary paleoceanography of the South China Sea: Glacial-interglacial contrasts in enclosed basin, *Paleoceanography, 5(1)*, 77-90, 1990.

Wang, L., M. Sarnthein, H. Erlenkeuser, J. Grimalt, P. Grootes, S. Heilig, E. Ivanova, M. Kienast, C. Pelejero, and U. Pflaumann, East Asian monsoon climate during the Late Pleistocene: High-resolution sediment records from the South China Sea, *Mar. Geol., 156(1-4)*, 245-284, 1999.

Wang, P., Response of West Pacific marginal seas to glacial cycles: Paleoceanographic and sedimentological features, *Mar. Geol., 156(1-4)*, 5-39, 1999.

Wang, P., and X. Sun, Last Glacial Maximum in China: Comparison between land and sea, *Catena, 23*, 341-353, 1995.

Wang, P., Q. Min, Y. Bian, and X. Cheng, On micropaleontology and stratigraphy of Quaternary marine transgressions in East China, in *Marine Micropaleontology of China*, edited by P. Wang, pp. 265-264, China Ocean Press, Beijing, 1985.

Wang, P., Q. Min, Y. Bian, and W. Feng, Planktonic foraminifera in the continental slope of the northern South China Sea during the last 130,000 years and their paleoceanographic implications, *Dizhi Xuebao*, 60, 1-11, 1986.

Wang, P., L. Wang, Y. Bian, and Z. Jian, Late Quaternary paleoceanography of the South China Sea: Surface circulation and carbonate cycles, *Mar. Geol., 127*, 145-165, 1995.

Weeks, R., C. Laj, L. Endignoux, M. Fuller, A. Roberts, R. Manganne, E. Blanchard, and W. Goree, Improvements in long-core measurements technique: Applications in paleomagnetism and paleoceanography, *Geophys. J. Int., 114*, 651-662, 1993.

Winn, K., L. Zheng, H. Erlenkeuser, and P. Stoffers, Oxygen/carbon isotopes and paleo-productivity in the South China Sea during the past 110,000 years, in *Marine Geology and Geophysics of the South China Sea*, edited by X. Jin, H.R. Kudrass, and G. Pautot, pp. 154-166, China Ocean Press, Beijing, 1992.

Wu, X., F. Jiang, S. Wang, and B. Xue, On the problem of the Yellow River cutting the Sanmen Gorge and flowing eastward into the sea (in Chinese), *Quat. Sci. Beijing, 2*, 188, 1998.

Wu, X., H. Xu, J. Deng, W. Yin, Z. Zen, H. Zheng, and Z. Ouyang, Records of two astrogeologic events in the loess strata, Lantian, Shaanxi, China, *Chin. Sci. Bull., 37(11)*, 946-950, 1992.

Wyrtki, K., *Physical oceanography of the Southeast Asian waters, scientific results of marine investigations of the South China Sea and the Gulf of Thailand 1959-1961, NAGA Rep. 2*, 195pp., Scripps Inst. Oceanogr., La Jolla, Calif., 1961.

Yan, X., C. Ho, Q. Zheng, and V. Klemas, Temperature and size variabilities of the western Pacific warm pool, *Science, 258*, 1643-1645, 1992.

Yang, Z., H. Lin, B. Tang, and W. Xue, Correlation of Quaternary event stratigraphy of shelf areas in the Asia—Pacific region, in *Research of Marine Geology and Mineral Resources*, edited by Inst. of Mar. Geol., MGMR, pp. 68-82, Qingdao Ocean Univ. Press, Qingdao, China, 1996.

Yasuda, M., W. H. Berger, G. Wu, S. Burke, and H. Schmidt, Foraminifera preservation record for the last million years: Site 805, Ontong Java Plateau. *Proc. Ocean Drill. Program Sci. Results, 130*, 491-508, 1993.

Zhang, M., A. Chivas, X. Wang, J. Liu, S. Li, and B. Liu, A study diagenesis of reef succession in Well Xichen-1, Xisha Islands, in *Research of Marine Geology and Mineral Resources*, edited by Inst. of Mar. Geol., MGMR, pp. 130-148, Qingdao Ocean Univ. Press, Qingdao, China, 1996.

Zhao, Q., Z. Jian, B. Li, X. Cheng, and P. Wang, Middle Pleistocene microtektites in deep-sediments of the South China Sea, *Sci. China Ser. D, 42(5)*, 531-535, 1999.

Y. Bian, X. Cheng, P. Wang, R. Wang, and Q. Zhao, Laboratory of Marine Geology, Tongji University, Shanghai 200092, China.

C. Bühring, Z. Jian, and U. Pflauman, Institut für Geowissenschaften, Universität Kiel, D-24118 Kiel, Germany. (zj@zaphod.gpi.uni-kiel.de)

M.-P. Chen, Institute of Oceanography, Taiwan University, Taipei, China.

C. Laj, Laboratoire des Sciences du Climat et de l' Environment, CNRS-CEA, 91198 Gif sur Yvette, France.

B. Li, Nanjing Institute of Geology and Paleo-ntology, Academia Sinica, Nanjing 210008, China.

H.-L. Lin, Institute of Marine Geology, Sun Yat-Sen University, Kaohsiung, Taiwan 804, China.

(Received July 30, 1999;
revised December 21, 1999;
accepted January 5, 2000.)